Al-Qadisiyah JournalFor Engineering Sciences 19 (2026) 153 – 163

Contents lists available at: http://qu.edu.iq

Al-Qadisiyah Journal for Engineering Sciences

Journal homepage: https://qjes.qu.edu.iq

Research Paper

Insights of Joule heating and chemical reaction effects on Casson-Williamson fluid in a thermally active Darcy–Forchheimer medium

Vardireddy Sujatha [1], ***Wuriti Sridhar*** [1]✉, ***Mohammed Abu-Ghurban*** [2]
Ganugapati R. Ganesh [3], ***G. Dharmaiah*** [4]

[1]*Department of Mathematics, Koneru Lakshmaiah Educational Foundation, Vaddeswaram, Guntur, 522302, India.*
[2]*College of Technical Engineering, Imam Ja'afar Al-Sadiq University, Al-Muthanna, 66001, Iraq.*
[3]*Department of Mathematics, PVP Siddhartha Institute of Technology, Kanuru, Vijayawada, A.P.520007, India.*
[4]*Department of Mathematics, Vasireddy Venkatadri International Technological University, Uppalapadu, Nambur, Guntur, A.P. 522508, India.*

ARTICLE INFO

Article history:
Received 24 September 2025
Received in revised form 14 December 2025
Accepted 23 February 2026

keyword:
Joule heating
Radiation
Chemical reaction
Porous media
Heat source
Darcy-Forchheimer media

ABSTRACT

This work examines the two-dimensional continuous flow of a Casson-Williamson fluid over a stretched surface under a Darcy-Forchheimer permeable medium. Several elements can affect the flow, including Joule heating, radiation, chemical reactions, thermal sources, electric field influences, and magnetic field influences. Nonlinear partial differential equations articulate the fundamental equations governing the system's dynamics in this physical model. We simplify these equations to a system of nonlinear ordinary differential equations by applying requisite changes. The Keller Box technique is utilized to simplify this collection of ordinary differential equations. Velocity, temperature and concentration graphs are plotted. The velocity profiles decline with a rise in the Casson parameter, magnetic parameter, porous parameter, Weissenberg number, and velocity slip parameter. Still, the electric field parameter diminishes when the speed slip constraint is enhanced. This study primarily examines several local properties, including the skin resistance coefficient, the Nusselt number, and the Sherwood numbers. We compare our results with the current literature by computing the skin friction coefficient for different inputs of the Casson factor. Prior studies have yielded results that are fairly congruent with this one.

1. Introduction

Numerous potential engineering uses are associated with fluid mechanics, which include the inquiry of temperature, fluid flow and mass transport. Some potential uses for this phenomenon include heat exchangers, cooling towers, refrigeration systems, heating and ventilation systems, and thermal control of electrical equipment. Currently, the flow of non-Newtonian fluids has garnered significant attention from researchers due to their increasing applications in industry and technology. Numerous scholars have investigated this type of fluid across various fields. Vajravelu et al. [1] explored the Casson liquid, demonstrating compared to Newtonian liquid behavior. After analyzing the impact of permeability, they concluded that the flux within the tube diminishes. Mustafa and associates [2] subsequently analyzed Casson liquid's time-dependent marginal sheet flow throughout a smooth sheet. As they elevated the values of the Casson constraint, the speed contours became increasingly steep. Research into Casson liquid flow over a permeable exterior influenced by an exponentially expanding dimension was carried out with the aid of Mukhopadhyay and colleagues [3]. As they expertly fine-tuned the Casson parameters, they decisively noted that the momentum border line sheet became remarkably slimmer. The compelling research by Makanda et al. [4] clearly specifies that elevated standards of both the unsteadiness restriction and the Casson restriction lead to a significant reduction in the speed profile of liquid flow across a time-varying extending surface within a permeable medium exhibiting magnetohydrodynamic (MHD) effects. Researchers Pushpalatha et al. [5] confidently established that a rise in the pressure constraint dramatically boosts the temperature and mass transport rates in Casson fluid flows subjected to convective border line requirements. Their rigorous investigation unequivocally led them to this groundbreaking finding through precise numerical analysis. Over time, the viscosity of Williamson fluid can change in a variety of ways. The viscosity of a Williamson fluid can be expressed by stating the shear stress and shear rate of the liquid as a linear relationship. This relationship can also be used to express the viscosity of the fluid. The construction business, the polymer industry, the food processing sector, and the personal care items industry are only some industries that use it. It is possible for engineers and researchers to have an improved comprehensive of and the ability to foresee the behaviour of complicated fluids by utilizing the Williamson fluid model, which enables the design and optimization of a wide variety of processes and products. The implementation of this is made feasible by the Williamson fluid model. Their analysis examines the behavior of Williamson fluid over a surface subjected to exponential stretching. Nadeem and Hussain [6] found that lower skin friction is obtained as the Williamson parameter is increased. Researchers Hayat et al. [7] found that the velocity field diminishes for Williamson fluid flow on a stretching surface as the attractive constraint improves. One of the things that came out of their inquiry was this. It was found that this phenomenon was caused by radiation and ohmic dissipation. The temperature profile rose, as Megahed [8] discovered while studying Williamson liquid stream influence over a nonlinear stretched exterior. This occurred as a result of the stimulus of energy and viscid dissipation, which increased the Williamson, viscosity, and thermal radiation parameters.

*Corresponding Author.
E-mail address: sridharwuriti@gmail.com ; Tel: (+91) 944-105 1978 (Wuriti Sridhar)

https://doi.org/10.30772/qjes.2025.165491.1749
2411-7773

Nomenclature			
B_0	Uniform magnetic field (T)	k^*	Mean absorption coefficient
C	Fluid concentration	q_r	The radiative heat flux
C_w	Nanoparticle concentration	q_w	The wall heat flux
C	Ambient value of the nanoparticle fraction	u, v	Velocity components
D_B	Brownian diffusion coefficient (m^2/s)	x, y	Space coordinates
D_T	Thermophoresis diffusion coefficient	We	Weissenberg parameter
E_C	Eckert number	α	Thermal diffusivity
N_b	Brownian motion parameter	β	Casson fluid parameter
N_t	Thermophoresis parameter	c	Coefficient of expansion with concentration
Pr	Prandtl number	β_T	Coefficient of thermal expansion
Fr	Forchhiemer parameter(dimensionless)	ρ_f	Fluid density (kg/m^3)
Δ	Mixed convection parameter	ν	Kinematic viscosity (m^2/s)
Q	Heat generation/absorption coefficient	μ	Dynamic viscosity of fluid, $kg/(m\ s)$
Q_0	Volumetric heat generation/ absorption (W/m^3)	σ	Electrical conductivity
R	Radiation parameter	σ^*	Stefan-Boltzman constant
T	Fluid temperature	γ	Chemical reaction parameter
T_w	Wall temperature	θ	Dimensionless temperature
T_∞	Ambient value of temperature	η	Dimensionless variable
k	Thermal conductivity, $W/(m\ K)$	$\lambda 1$	Slip Parameter
k_0	Chemical reaction coefficient	E_o	Electric field strength (V/m)

Ramzan et al. [9] determined that the velocity of nanoliquid particles decreases with a rise in the nanoparticle volume fraction. This conclusion was drawn following their analysis of Williamson Ferro nanofluid across an extended sheet. Zhu et al. [10] carried out an investigation into the thermal and dimension transport properties of Williamson nanofluid flow over a spreading page, while also considering the effects of Brownian motion and thermophoresis. Among the factors studied, they found that mass transfer amplified as the values of the Weissenberg number increased. Priyadarshini et al. [11] undertook a further study examining the encouragement of bio-convection on the flow of Williamson fluid over a symmetrical stretched sheet. They identified a correlation between the Prandtl number and the radiation parameter, noting an increase in the Nusselt number. The flow of Williamson nanofluid, impacted by frictional warming and sticky dissipation, was analyzed by Arif et al. [12], who found that the warmth describe rises in accordance with the increase of the Eckert number. A system that releases thermal energy into the atmosphere around it is referred to as a heat source. The utilization of heat sources in industrial settings is essential for a variety of specific applications. It has a expansive bounds of submissions in several application spheres. Among other things are research on nuclear fusion, MHD generators, magnetic medication delivery, and so on. In addition, the food and beverage business, the metallurgical sector, the water treatment industry, and the energy generation industry all have significant applications for chemical reactions. Within the context of a stretching slippery curved melting sheet, Kumar et al. [13, 14] conducted a study on Casson Williamson nanofluid. They found that the current buoyancy element contributes to enhancing speed profiles. The behavior of Williamson-Casson nanofluid flow across an extending piece was examined in a subsequent work. Their investigation indicates that the Brownian motion parameter is significantly improved when melting, thermophoresis, and Brownian motion all influence the temperature profile; their research assessed the influence of biological responses on the current of Casson-Williamson nanofluids across a slippery overextended exterior. Yousef et al. [15] demonstrated that elevating the temperatures of the slip velocity parameter, the Casson parameter, and the nanofluids themselves significantly boosts flow dynamics. Kazaz, Oguzhan, and Eiyad Abu-Nada [16] examined a new thermal fluid that can act as an efficient solar absorber and investigated that advance heat transfer fluids enhance solar evaporation rate. Hassan et al. [17] investigated fluid structure investigation and heat transfer characteristics of nano-encapsulated phase change material using the arbitrary Lagrangian Eulerian technique, and noted that NEPCM volume concentration strongly enhances heat transfer. In a subsequent investigation, Kazaz, Oguzhan, and Eiyad Abu-Nada [18] developed a new composite phase change nanomaterial which is utilized for thermal storage of solar radiation. Nazeer et al.[19] examined the phase flow of Jeffery fluid and observed that the momentum of Jeffery fluid increases gradually due to the Darcy number. Hussain et al. [20] studied Casson fluid flow with the influence of gravitational and magnetic forces through a uniformly inclined channel, thermal profile declines with the magnetic field's strength. Saleem et al. [21] investigated Ellis nanofluid flow in a wavy channel and concluded viscous dissipation is more dominant than heat conduction. Irfan et al. [22] examined the Ellis nanofluid model with a single-walled carbon tube and its applicability in the biomedical field. Islam et al. [23] examined triple diffusive fluid flow over a stretching surface using the Runge-Kutta scheme and observed that augmented observations of the Lewis number lower the heat and mass transfer rates. Nazeer et al. [24, 25] examined two-phase Williamson fluid flow through a tilted channel using the perturbation method, also analyzed blood gold Casson fluid through a wavy channel and observed that the shape of the particle is crucial in entropy generation. Almutairi et al. [26] studied multiphase flow of a Williamson fluid through convergent and divergent conduits and observed that the Weissenberg number decays the velocity distribution.Irfan et al.[27] studied Casson nanofluid through an asymmetric channel and highlighted the usage of different types of nanoparticles to achieve maximum heat enhancement. Later, Hussain et al. [28] Casson fluid flows through a vertical channel and observed that both porous and solid volume fraction parameters decline the fluid's velocity and temperature distribution. In a subsequent investigation, Abbas et al. [29] analyzed the Casson-Williamson fluid flow through a permeable medium on a slippery surface. Their findings unmistakably showed that the skin friction coefficient escalates as the porosity parameter increases, while the momentum boundary thickness contracts with elevated slip parameter values. Alomari et al. [30] examined the Convection flow of NE-phase change material-water mixture in evacuated tube solar collector manifold: Numerical analysis of MHD double-diffusive convection and exothermic reaction. Bilal Ali et al. [31] examined the numerical modelling and deep learning-based analysis of unsteady micropolar nanofluid flow with heat radiation over a rigid plate. This research investigates the mass transfer and flow behaviour of Casson–Williamson fluids over a stretching surface while accounting for multiple interacting physical effects, including chemical reaction, Joule heating, viscous dissipation, porosity, MHD forces, electric field, and internal heat generation. The theoretical formulation and numerical analysis emphasise how current conduction mechanisms influence the steady flow of a Casson–Williamson fluid over an impermeable stretched sheet. By incorporating Ohmic heating, Joule heating, and homogeneous chemical reaction into a unified model and solving it using the Keller Box method, the study provides a comprehensive evaluation of the governing transport processes.The novelty of this work lies in presenting, for the first time, a combined theoretical and numerical investigation of Casson–Williamson fluid flow over a Darcy–Forchheimer porous stretched sheet that simultaneously includes Joule heating, chemical reaction, and current-conduction effects. This unique combination of fluid rheology, porous-medium modelling, and thermophysical interactions has not been previously reported in the literature and forms the central contribution of the present study.

2. Problem formulation

In this article, a two-dimensional continuous Casson-Williamson liquid flow through a stretched sheet is considered mentioned in Fig. 1. The stretched sheet is regarded to be in the control of the x-axis, and the y-axis is normal to the surface. Within the scope of this investigation, attributes such as porous medium, electrical field, heat source, joule heating, thermal radiation, and chemical reaction characteristics were taken into consideration. The extending sheet speed is considered as $U_w = ax$. These assumptions lead to the governed flow, momentum, energy and concentration equations of the study that are shown below Eqs. 1, 2, 3 and Eq. 4 respectively [15, 29].
In Eq. 2 first term represents momentum diffusion term, second term represents Williamson fluid shear dependent viscosity term, In third term $\frac{\sigma}{\rho}(E_o B_o)$

represents electro magnetic driving force, and the term $-\frac{\sigma}{\rho}(B_o^2 u)$ represents Magnetic damping term. Also the term $-\frac{v}{k}u$ represents darcy resistance term. the $\frac{C_b}{\sqrt{k_o}}u^2$ represents Forchhiemer inertial parameter, and $g\beta^*(T-T_\infty)$ represents buoyancy term.

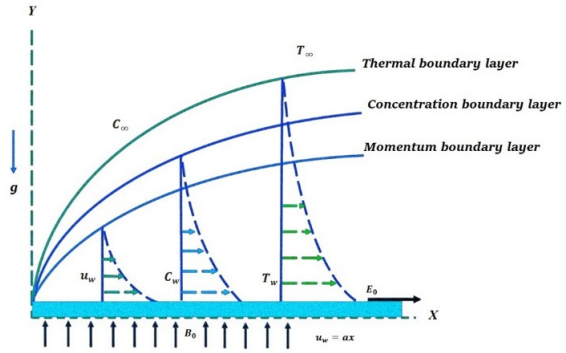

Figure 1. Flow model of the problem.

In Eq. 3 L.H.S term represents convective heat transport, right hand side first term represent viscous dissipation term , second term represents thermal diffusion and radiation term, next term represents electromagnetic heating term and last term represents heat source. In the absence of together, Casson restriction(β) and Time constant constraint(Γ) Newtonian model case can be obtained. Here in the boundary conditions velocity slip factor(λ_1) is considered. In Eq. 5, the first term represents the velocity profile at the wall, and the second terms represent nonlinear slip effects. The T_w,C_w represents temperature and concentration of the wall. The T_∞, C_∞ represent ambient temperature and concentration, respectively. Similarity transformations used are Eq. 6.

$$\frac{\partial u}{\partial x}+\frac{\partial v}{\partial y}=0 \tag{1}$$

$$v\left(1+\frac{1}{\beta}\right)\frac{\partial^2 u}{\partial y^2}+\sqrt{2}v\Gamma\frac{\partial u}{\partial y}\frac{\partial^2 u}{\partial y^2}+\frac{\sigma}{\rho}\left(E_o B_o-B_o^2 u\right)-\frac{v}{k}u-\frac{C_b}{\sqrt{k_o}}u^2+ +g\beta^*(T-T_\infty)=u\frac{\partial u}{\partial x}+v\frac{\partial v}{\partial y} \tag{2}$$

$$u\frac{\partial T}{\partial x}+v\frac{\partial T}{\partial y}=\frac{\mu}{\rho c_p}\left[\left(1+\frac{1}{\beta}\right)\left(\frac{\partial u}{\partial y}\right)^2+\frac{\Gamma}{\sqrt{2}}\left(\frac{\partial u}{\partial y}\right)^3\right]+\frac{k}{\rho c_p}\left(1+\frac{16\sigma^* T_\infty^3}{3kk^*}\right)\frac{\partial^2 T}{\partial y^2}+\frac{\sigma}{\rho c_p}(uB_o-E_o)^2+\frac{Q_o}{\rho c_p}(T-T_\infty) \tag{3}$$

$$D_B\frac{\partial^2 C}{\partial y^2}-k_1(C-C_\infty)=u\frac{\partial C}{\partial x}+v\frac{\partial C}{\partial y} \tag{4}$$

Thus, using the following boundary conditions, Eq. 5, [16, 30].

$$\left.\begin{aligned} &u=ax+\lambda_1\left[\left(1+\frac{1}{\beta}\right)\frac{\partial u}{\partial y}+\frac{\Gamma}{\sqrt{2}}\left(\frac{\partial u}{\partial y}\right)^2\right]\Rightarrow at\ y=0\\ &v=0, T=T_w, C=C_w\Rightarrow at\ y=0\\ &\{u\to 0, T\to T_\infty, C\to C_\infty\}\Rightarrow\ \ as\ \ y\to\infty \end{aligned}\right\} \tag{5}$$

$$\left.\begin{aligned} &u=axf'(\eta)\\ &v=-\sqrt{av}f(\eta)\\ &\theta=\frac{T-T_\infty}{T_w-T_\infty}\\ &\phi=\frac{C-C_\infty}{C_w-C_\infty}\\ &\eta=y\frac{a}{v} \end{aligned}\right\} \tag{6}$$

Where $u=axf'(\eta)$ represents streamwise velocity, $v=-\sqrt{av}f(\eta)$ represents normal velocity which gives the suction/blowing structure of the boundary layer from continuity equation. $\theta=\frac{T-T_\infty}{T_w-T_\infty}$ represents temperature transformation and $\phi=\frac{C-C\infty}{C_w-C_\infty}$ represents concentration transformation. $\eta=y\sqrt{\frac{q}{v}}$ represents similarity variable. All the above transformations are used to convert governing partial differential equations to set of ordinary differential equations. Using the transformations mentioned in Eq. 6 equations are transformed to Eqs. 7, 8 and 9.

$$\left(\left(1+\frac{1}{\beta}\right)+We f''\right)f'''-f'^2- -M(E_1)+(M-k_p)f'-Frf'^2+ff''+\Delta\theta=0 \tag{7}$$

$$\theta''(1+\varepsilon\theta)+\varepsilon\theta'^2+\frac{3PrJ}{3+4Rd}\left(f'-E_1\right)^2+\frac{3PrJ}{3+4Rd}f\theta'+ +\frac{3PrEcJ}{3+4Rd}\left(\left(1+\frac{1}{\beta}\right)f''^2+\frac{We}{2}f''^3\right)+\frac{3PrQ}{3+4Rd}\theta=0 \tag{8}$$

$$\theta''+Scf\phi'-Sc\Gamma\phi=0 \tag{9}$$

Also using transformations 6, the BC's 5 are converted to Eq. 10.

$$\left.\begin{aligned} &f(\eta)=0, f'(\eta)=1+\lambda f''\left[\left(\frac{\beta+1}{\beta}\right)+\frac{We}{2}f''\right]\\ &\theta(0)=1,\phi(0)=1\ \ at\ \eta=0\\ &f'(\eta)\to 0,\theta(\eta)\to 0,\phi(\eta)\to 0\ \ as\ \eta\to\infty \end{aligned}\right\} \tag{10}$$

Where $M=\frac{\sigma B_o^2}{\rho a}$, $We=\Gamma\sqrt{\frac{a}{v}}$, $E_1=\frac{E_o}{B_o\sqrt{av}}$, $k_p=\frac{v}{k\times a}$, $Fr=\frac{C_b}{\sqrt{k^*}}\Delta=\frac{g\beta_T(T_W-T_\infty)}{a\sqrt{av}}$, $Pr=\frac{v\rho c_p}{k}$, $Ec=\frac{av}{c_p(T_W-T_\infty)}$, $Rd=\frac{16\sigma^* T_\infty^3}{3kk^*}$, $Q=\frac{Q_o v}{ka(T_W-T_\infty)}$, $Sc=\frac{v}{D_B}$, and $\Gamma=\frac{k_1}{a}$

3. Numerical methodology

The governing partial differential equations are solved using Keller Box method using the procedure described below Fig. 2.

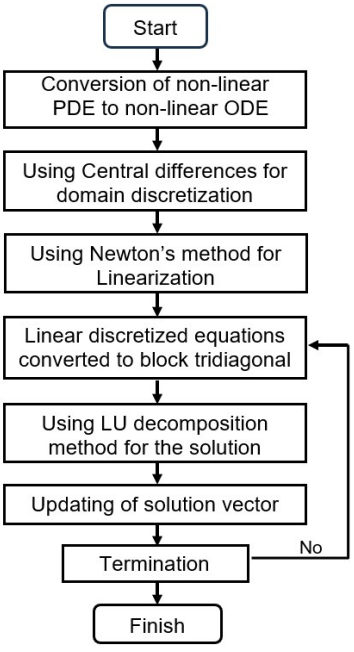

Figure 2. Flow chart.

Introducing new variables, $\frac{df}{d\eta} = p$, $\frac{dp}{d\eta} = q$, $g = \theta$, $t = \frac{dg}{d\eta}$, $S = \phi$, and $n = \frac{ds}{d\eta}$, the nonlinear Eqs. 7, 8 and 9 are changed to Eqs. 11, 12 and 13.

$$q' + \left(\frac{\beta}{\beta+1}\right)\left(weqq' + fq - p^2 - ME_1 + Mp - k_p p - Frp^2 + Ag\right) = 0 \tag{11}$$

$$t' + \varepsilon g t' + \varepsilon t^2 + \frac{3PrJ}{3+4Rd}p^2 + \frac{3PrJE_1^2}{3+4Rd} - \frac{6PrJE_1}{3+4Rd}p + \frac{3PrJ}{3+4Rd}ft + \frac{3PrEcJ}{3+4Rd}\left(1+\frac{1}{\beta}\right)q^2 + \frac{3PrEcWeJ}{2(3+4Rd)}q^3 + \frac{3PrQ}{3+4Rd}q = 0 \tag{12}$$

$$n' + Scfn - Sc\Gamma S = 0 \tag{13}$$

Introducing the concept of finite differences, Newton's method, the set of equations we get is 14.

$$\left.\begin{aligned}
&\delta f_k - \frac{h_k}{2}\delta p_k - \frac{h_k}{2}\delta p_{(k-1)} - \delta f_{(k-1)} = (r_1)_k\\
&\delta p_k - \frac{h_j}{2}\delta q_k - \frac{h_k}{2}\delta q_{(k-1)} - \delta p_{(k-1)} = (r_2)_k\\
&\delta g_k - \frac{h_j}{2}\delta t_k - \frac{h_k}{2}\delta t_{(k-1)} - \delta g_{(k-1)} = (r_3)_k\\
&\delta s_k - \frac{h_j}{2}\delta n_k - \frac{h_j}{2}\delta n_{(k-1)} - \delta s_{(k-1)} = (r_4)_k\\
&(a_1)_k\delta q_k + (a_2)_k\delta q_{(k-1)} + (a_3)_k\delta f_k + (a_4)_k\delta f_{(k-1)} + (a_5)_k\delta p_k + (a_6)_k\delta p_{(k-1)} + (a_7)_k\delta g_k + (a_8)_k\delta g_{(k-1)} = (r_5)_k\\
&(b_1)_k\delta t_k + (b_2)_k\delta t_{(k-1)} + (b_3)_k\delta g_k + (b_4)_k\delta g_{(k-1)} + (b_5)_k\delta p_k + (b_6)_k\delta p_{(k-1)} + (b_7)_k\delta f_k + (b_8)_k\delta f_{(k-1)} + (b_9)_k\delta q_k + (b_{10})_k\delta q_{(k-1)} = (r_6)_k\\
&(c_1)_k\delta n_k + (c_2)_k\delta n_{(k-1)} + (c_3)_k\delta f_k + (c_4)_k\delta f_{(k-1)} + (c_5)_k\delta s_k + (c_6)_k\delta s_{(k-1)} = (r_7)_k
\end{aligned}\right\} \tag{14}$$

Where the a_i, b_i, c_i and r_i are shown in Eqs. 15, 16, 17 and 18.

$$\left.\begin{aligned}
(a_1)_k &= 1 + \frac{\beta We}{2(\beta+1)}(q_k+q_{k-1}) + \frac{\beta We}{2(\beta+1)}(q_k-q_{k-1}) - \frac{\beta h_k}{4(\beta+1)}(f_k-f_{k-1})\\
(a_2)_k &= -1 - \frac{\beta We}{2(\beta+1)}(q_k+q_{k-1}) + \frac{\beta We}{2(\beta+1)}(q_k-q_{k-1}) - \frac{\beta h_k}{4(\beta+1)}(f_k-f_{k-1})\\
(a_3)_k &= \frac{\beta h_k}{4(\beta+1)}(q_k+q_{k-1})\\
(a_4)_k &= \frac{\beta h_k}{4(\beta+1)}(q_k+q_{k-1})\\
(a_5)_k &= \frac{-\beta h_k}{2(\beta+1)}(p_k+p_{k-1}) + \frac{M\beta h_k}{2(\beta+1)} - \frac{k_p\beta h_k}{2(\beta+1)} - \frac{Fr\beta h_j}{2(\beta+1)}(p_j+p_{j-1})\\
(a_6)_k &= \frac{-\beta h_k}{2(\beta+1)}(p_k+p_{k-1}) + \frac{M\beta h_k}{2(\beta+1)} - \frac{k_p\beta h_k}{2(\beta+1)} - \frac{Fr\beta h_j}{2(\beta+1)}(p_j+p_{j-1})\\
(a_7)_k &= \frac{\Delta\beta h_k}{2(\beta+1)}\\
(a_8)_k &= \frac{\Delta\beta h_k}{2(\beta+1)}
\end{aligned}\right\} \tag{15}$$

$$\left.\begin{aligned}
(b_1)_k &= 1 + \frac{\varepsilon}{2}(g_k+g_{k-1}) + \frac{\varepsilon h_k}{2}(t_k+t_{k-1}) + \frac{3Prh_k}{4(3+4Rd)}(f_k-f_{k-1})\\
(b_2)_k &= -1 - \frac{\varepsilon}{2}(g_k+g_{k-1}) + \frac{\varepsilon h_k}{2}(t_k+t_{k-1}) + \frac{3Prh_k}{4(3+4Rd)}(f_k-f_{k-1})\\
(b_3)_k &= \frac{\varepsilon}{2}(t_k+t_{k-1}) + \frac{3PrQh_k}{2(3+4Rd)}\\
(b_4)_k &= \frac{\varepsilon}{2}(t_k+t_{k-1}) + \frac{3PrQh_k}{2(3+4Rd)}\\
(b_5)_k &= \frac{3PrJh_k}{4(3+4Rd)}(t_k+t_{k-1}) - \frac{3PrJE_1h_k}{3+4Rd}\\
(b_6)_k &= \frac{3PrJh_k}{4(3+4Rd)}(t_k+t_{k-1}) - \frac{3PrJE_1h_k}{3+4Rd}\\
(b_7)_k &= \frac{3Prh_k}{4(3+4Rd)}(t_k+t_{k-1})\\
(b_8)_k &= \frac{3Prh_k}{4(3+4Rd)}(t_k+t_{k-1})\\
(b_9)_k &= \frac{3PrEc(\beta+1)h_k}{2\beta(3+4Rd)}(q_k+q_{k-1}) + \frac{3PrEcWeh_j}{16(3+4Rd)}(q_k+q_{k-1})^2\\
(b_{10})_k &= \frac{3PrEc(\beta+1)h_k}{2\beta(3+4Rd)}(q_k+q_{k-1}) + \frac{3PrEcWeh_j}{16(3+4Rd)}(q_k+q_{k-1})^2
\end{aligned}\right\} \tag{16}$$

$$\left.\begin{aligned}
(c_1)_k &= 1+\frac{Sch_k}{4}(f_k+f_{k-1})\\
(c_2)_k &= -1+\frac{Sch_k}{4}(f_k+f_{k-1})\\
(c_3)_k &= \frac{Sch_k}{4}(n_k+n_{k-1})\\
(c_4)_k &= \frac{Sch_k}{4}(n_k+n_{k-1})\\
(c_5)_k &= \frac{-Sc\Gamma h_k}{2}\\
(c_6)_k &= \frac{-Sc\Gamma h_k}{2}
\end{aligned}\right\} \tag{17}$$

$$\left.\begin{aligned}
(r_1)_k &= f_{k-1}-f_k-\frac{h_k}{2}(p_k+p_{k-1})\\
(r_2)_k &= p_{k-1}-p_k-\frac{h_k}{2}(q_k+q_{k-1})\\
(r_3)_k &= g_{k-1}-g_k-\frac{h_k}{2}(t_k+t_{k-1})\\
(r_4)_k &= S_{k-1}-S_k-\frac{h_k}{2}(n_k+n_{k-1})\\
(r_5)_k &= q_{k-1}-q_k-\frac{\beta We}{2(\beta+1)}(q_k+q_{k-1})(q_k-q_{k-1})+\frac{\beta h_k}{4(\beta+1)}(p_k+p_{k-1})^2+\frac{M\beta E_1 h_k}{\beta+1}-\frac{M\beta h_k}{2(\beta+1)}(p_k+p_{k-1})+\frac{k_p\beta h_k}{2(\beta+1)}(p_k+p_{k-1})+\\
&\quad+\frac{Fr\beta h_k}{4(\beta+1)}(p_k+p_{k-1})^2-\frac{\Delta\beta h_k}{2(\beta+1)}(g_k+g_{k-1})-\frac{\beta h_k}{4(\beta+1)}(f_k+f_{k-1})(q_k+q_{k-1})\\
(r_6)_k &= t_{k-1}-t_k-\frac{\varepsilon}{2}(g_k+g_{k-1})(t_k-t_{k-1})-\frac{\varepsilon h_k}{4}(t_k+t_{k-1})^2-\frac{3PrJh_k}{4(3+4Rd)}(p_k+p_{k-1})^2-\frac{3PrJE_1^2h_k}{3+4Rd}+\frac{2PrJE_1h_k}{2(3+4Rd)}(p_k+p_{k-1})-\\
&\quad-\frac{3Prh_k}{4(3+4Rd)}(f_k+f_{k-1})(t_k+t_{k-1})-\frac{3PrEch_k}{4(3+4Rd)}\frac{\beta+1}{\beta}(q_k+q_{k-1})^2-\frac{3PrEcWeh_k}{16(3+4Rd)}(g_k+g_{k-1})^3-\frac{3PrQh_k}{2(3+4Rd)}(g_k+g_{k-1})\\
(r_7)_k &= n_{k-1}-n_k-\frac{Sch_k}{4}(f_k+f_{k-1})(n_k+n_{k-1})+\frac{Sc\Gamma h_k}{2}(S_k+S_{(k-1)})
\end{aligned}\right\} \tag{18}$$

The matrix form represented by the system are Eq. 19.

$$\left.\begin{aligned}
&[A_1][\delta_1]+[C_1][\delta_1]=[r_1]\\
&[B_1][\delta_1]+[A_2][\delta_2]+[C_2][\delta_3]=[r_2]\\
&....\\
&[B_{j-1}][\delta_1]+[A_{j-1}][\delta_2]+[C_{j-1}][\delta_3]=[r_{j-1}]\\
&[B_j][\delta_{j-1}]+[A_j][\delta_j]=[r_j]
\end{aligned}\right\} \tag{19}$$

Were the A_j, B_j and C_j matrices are Eq. 20.

$$[A_1]=\begin{pmatrix}
0 & 0 & 0 & 1 & 0 & 0 & 0\\
-\frac{h_j}{2} & 0 & 0 & 1 & -\frac{h_j}{2} & 0 & 0\\
0 & -\frac{h_j}{2} & 0 & 0 & 0 & -\frac{h_j}{2} & 0\\
0 & 0 & -1 & 0 & 0 & 0 & -\frac{h_j}{2}\\
(a_2)_1 & 0 & 0 & (a_3)_1 & (a_1)_1 & 0 & 0\\
(b_{10})_1 & (b_2)_1 & 0 & (b_7)_1 & (b_9)_1 & (b_1)_1 & 0\\
0 & 0 & (c_6)_1 & (c_3)_1 & 0 & 0 & (c_1)_1
\end{pmatrix}$$

$$[A_j]=\begin{pmatrix}
-\frac{h_j}{2} & 0 & 0 & 1 & 0 & 0 & 0\\
-1 & 0 & 0 & 0 & -\frac{h_j}{2} & 0 & 0\\
0 & -1 & 0 & 0 & 0 & -\frac{h_j}{2} & 0\\
0 & 0 & -1 & 0 & 0 & 0 & -\frac{h_j}{2}\\
(a_6)_j & (a_8)_j & 0 & (a_3)_j & (a_1)_j & 0 & 0\\
(b_6)_j & (b_4)_j & 0 & (b_7)_j & (b_9)_j & (b_1)_j & 0\\
0 & 0 & (c_6)_j & (c_3)_j & 0 & 0 & (c_1)_j
\end{pmatrix}$$

$$[B_j]=\begin{pmatrix}
0 & 0 & 0 & -1 & 0 & 0 & 0\\
0 & 0 & 0 & 0 & -\frac{h_j}{2} & 0 & 0\\
0 & 0 & 0 & 0 & 0 & -\frac{h_j}{2} & 0\\
0 & 0 & 0 & 0 & 0 & 0 & -\frac{h_j}{2}\\
0 & 0 & 0 & (a_4)_j & (a_2)_j & 0 & 0\\
0 & 0 & 0 & (b_8)_j & (b_{10})_j & (b_2)_j & 0\\
0 & 0 & (c_4)_j & 0 & 0 & 0 & (c_2)_j
\end{pmatrix}$$

$$[C_j]=\begin{pmatrix}
-\frac{h_j}{2} & 0 & 0 & 0 & 0 & 0 & 0\\
1 & 0 & 0 & 0 & 0 & 0 & 0\\
0 & 1 & 0 & 0 & 0 & 0 & 0\\
0 & 0 & 1 & 0 & 0 & 0 & 0\\
(a_5)_j & (a_7)_j & 0 & 0 & 0 & 0 & 0\\
(b_5)_j & (b_3)_j & 0 & 0 & 0 & 0 & 0\\
0 & 0 & (c_5)_j & 0 & 0 & 0 & 0
\end{pmatrix} \tag{20}$$

The *LU* decomposition technique is capable of determining the method's resulting block diagonal configuration. The computations are performed continuously until the specified coming together criteria are satisfied, and they are concluded while the value of $|\delta g_0^i| < \varepsilon$, which is exceedingly tiny, attains the suggested limit. Specifically, we report the average CPU time required for the Keller Box iterations and the observed convergence rate. For the present simulations, the Keller Box method typically converged within 4–6 iterations per step, with a residual tolerance of 10^{-6}.

4. Results and discussions

Casson parameter velocity profiles are depicted in Fig. 3. A steeper drop in the speed outline is the consequence of a larger Casson parameter, which causes the fluid's viscosity to rise. Figure 4 shows some Weissenberg parameter velocity profiles. As a function of retardation time, the Weissenberg number quantifies how long it takes for fluids to relax. A thicker fluid, which will cause the velocity profile to decline, and provide better Weissenberg number values. The electric field parameter's velocity profiles are graphically depicted in Fig. 5.

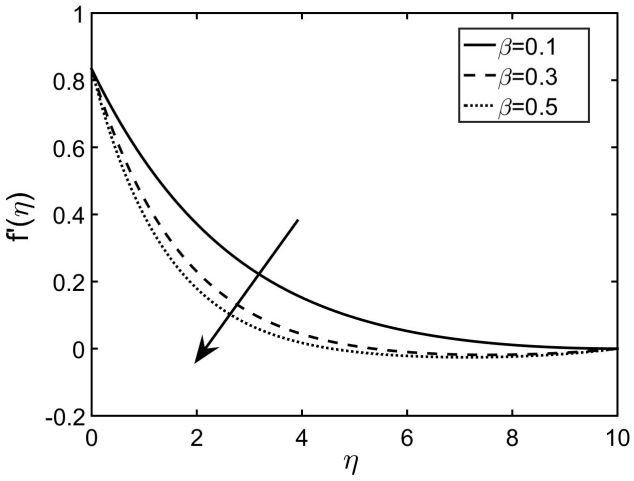

Figure 3. Variations of velocity with change in Casson Parameter.

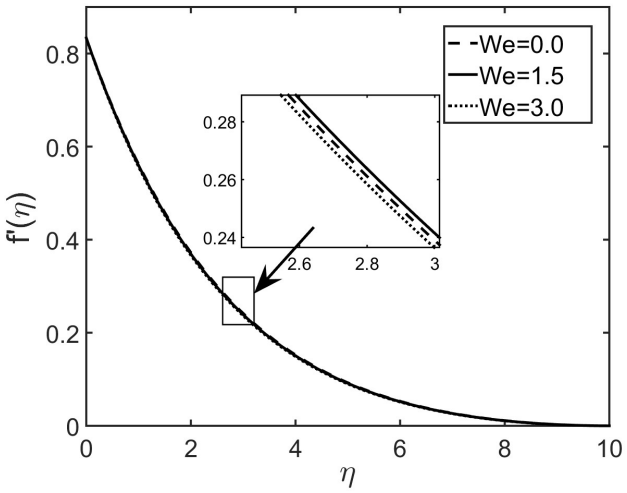

Figure 4. Variations of velocity with the change in Weissenberg parameter.

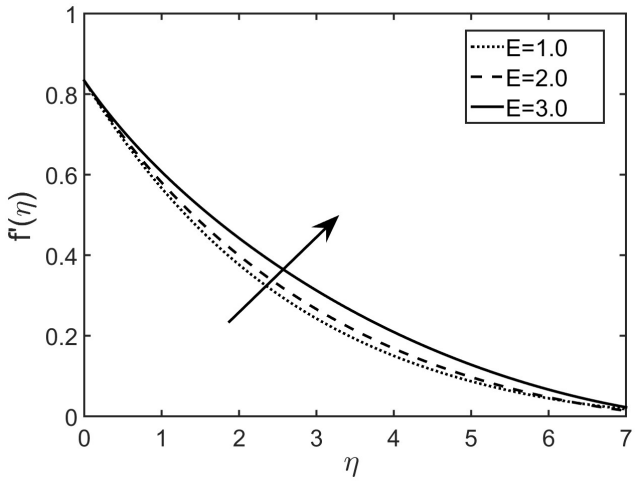

Figure 5. Variations of Speed with the change in Electric field parameter.

The measured velocity profile grows as the electric field parameter increases because a thicker boundary layer produces a force inside the liquid, indicating an electric field growth. In Fig. 6, we can see the magnetic parameter's velocity curve. The formation of an opposing force within a fluid is affected by an increase in the magnetic constraint, which decreases the fluid flow speed and, ultimately, causes the fluid velocity to decline. For the speed slip constraint, see Fig. 7 for an illustration of its speed outlines. As the speed slip-up constraint is improved, the velocity profile is lowered. In Fig. 8 for the porous parameter's velocity profiles. Reduced velocity profiles are the outcome of frictional force generation within the fluid layers caused by increased values of the porosity parameter.

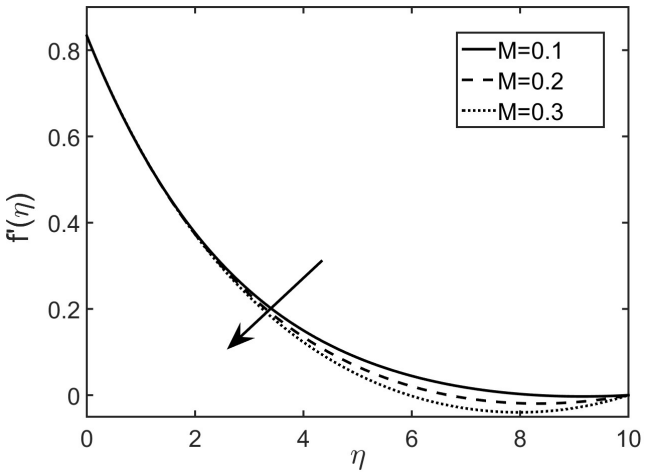

Figure 6. Variations of Velocity with the change in Magnetic parameter.

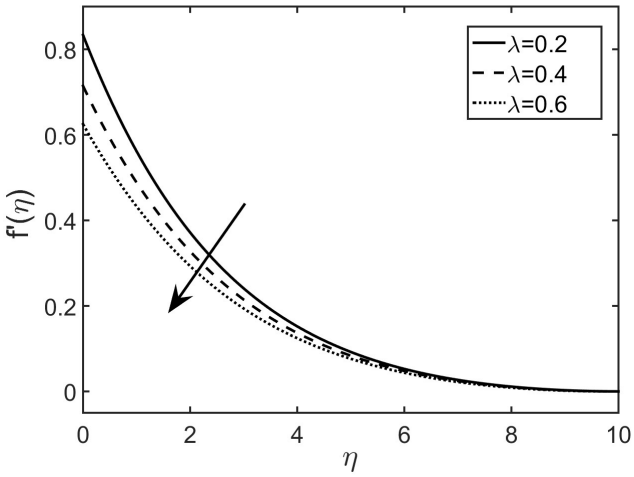

Figure 7. Variations of Velocity with the change in slip parameter.

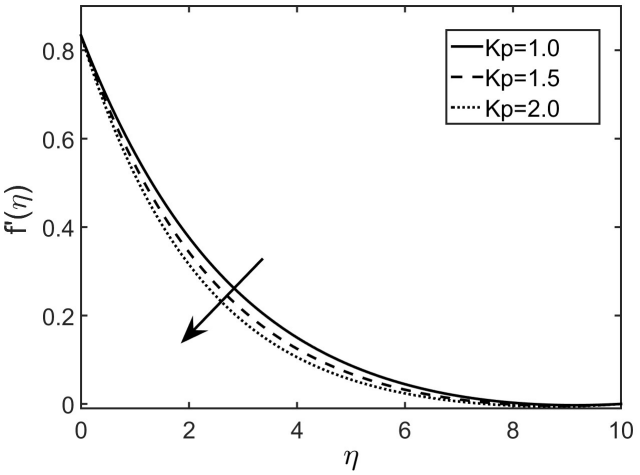

Figure 8. Variations of Velocity with the change in Porous parameter.

Increasing the Forchheimer parameter velocity decreases, which is depicted in Fig. 9. For elevated values of the Forchheimer parameter, a marked increase in resistance is observed, thereby leading to a decrease in the liquid flow speed. The Casson parameter's temperature profiles are illustrated in Fig. 10. As the width of the current borderline sheet increases, the temperature profiles significantly improve. Figure 11 presents the warmth profiles derived from the Weissenberg number. The warm outline becomes increasingly distinct with the rise of the Weissenberg number.

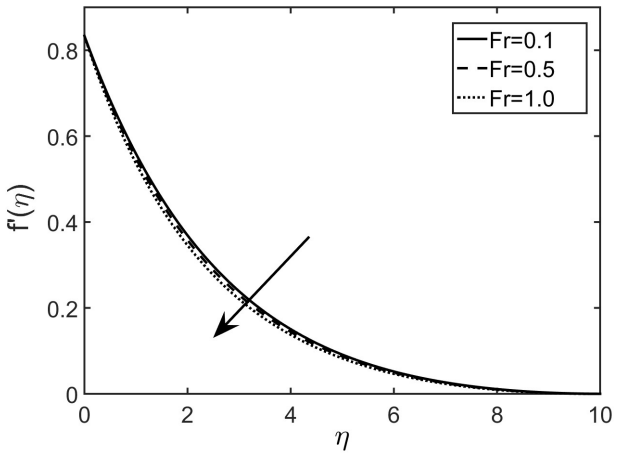

Figure 9**.** Variations of Velocity with the change in Forcchiemer parameter.

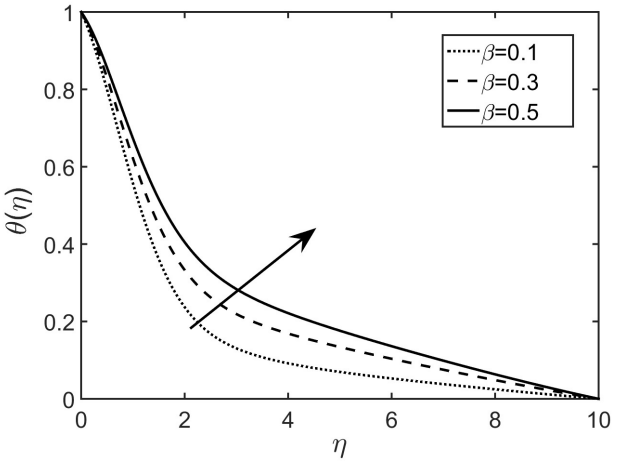

Figure 10**.** Variations of Temperature with the change in Casson constraint.

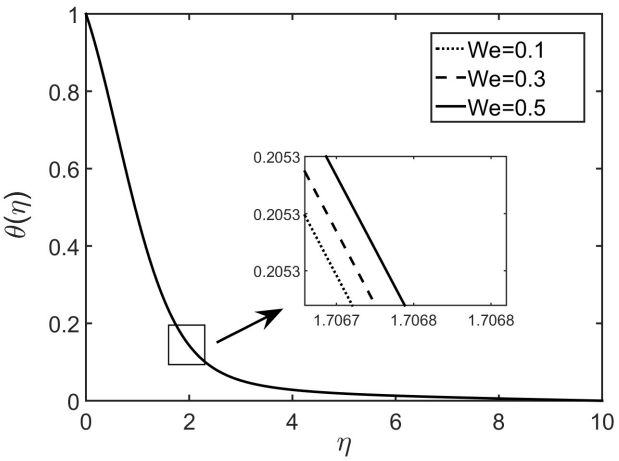

Figure 11**.** Variations of Temperature with the change in Weissenberg number.

In Fig. 12, the temperature profiles of the magnetic parameter are displayed. As the magnetic parameter is raised to higher values, the magnitude of velocity is reduced in the boundary layer; consequently, temperature in the boundary layer increases, so an upward shift in the temperature profile is observed because Lorentz force acts opposite to the flow, so to sustain same rate of flow internal work in the fluid causes heat dissipation.

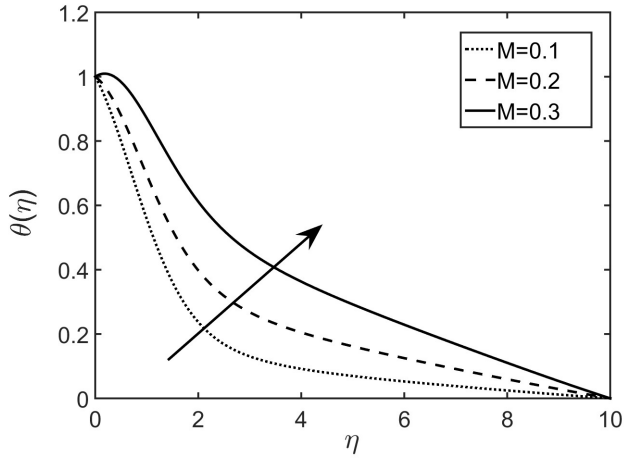

Figure 12**.** Variations of Temperature with the change in Magnetic parameter.

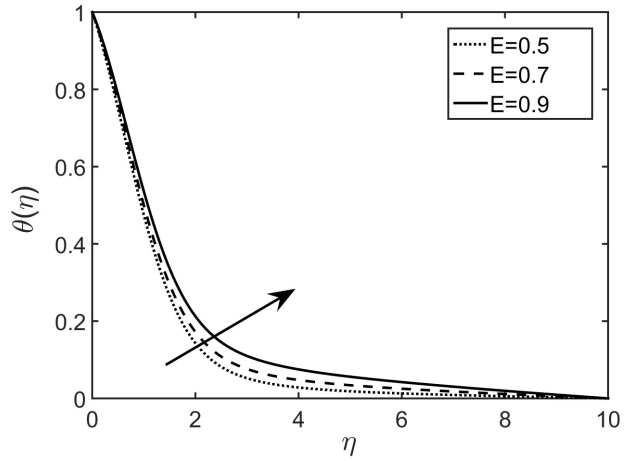

Figure 13**.** Variations of Temperature with the change in Electric field parameter.

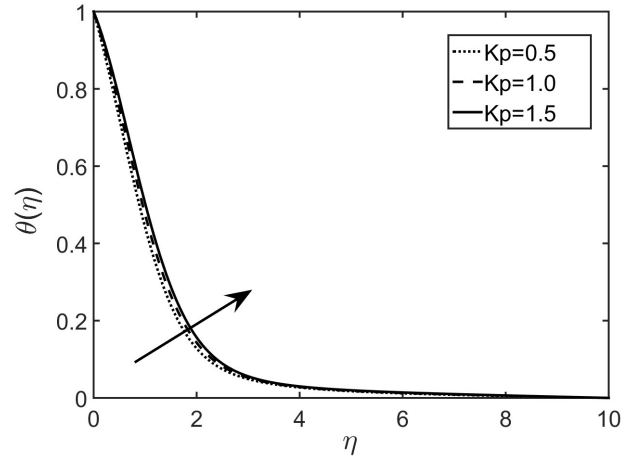

Figure 14**.** Variations of Temperature with the change in Porous parameter.

Figure 13 exhibits the distributions of temperatures for the electric field parameter. The warmth described is improved by doing extra electric field factor measurements because As a result of a stronger electric field, there are more charges able to move, which results in an increase in electrical resistance, which in turn causes the energy to be converted into heat. Figure 14 displays detailed temperature profiles of the porosity parameter.

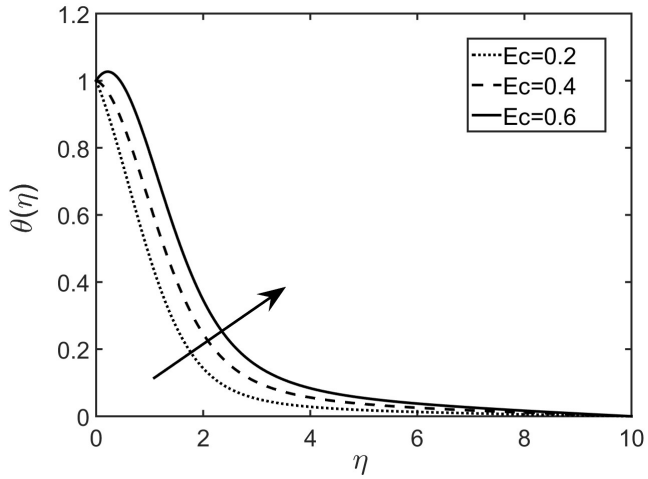

Figure 15**.** Variations of Temperature with the change in Eckert number.

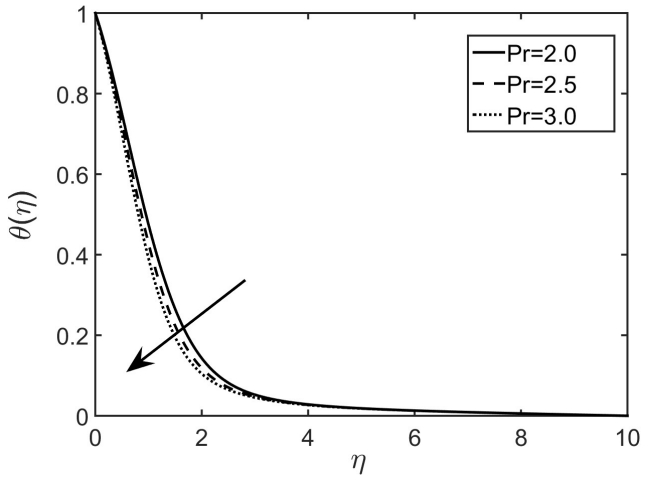

Figure 16**.** Variations of Temperature with the change in Prandtl number.

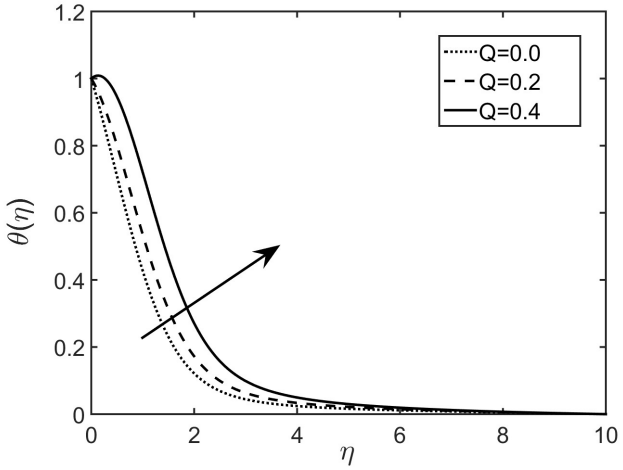

Figure 17**.** Variations of Temperature with the change in heat source parameter.

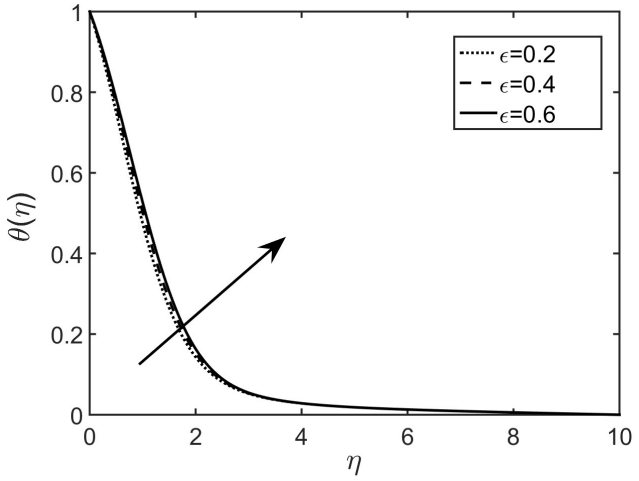

Figure 18**.** Variations of Temperature with the change in thermal conductivity parameter.

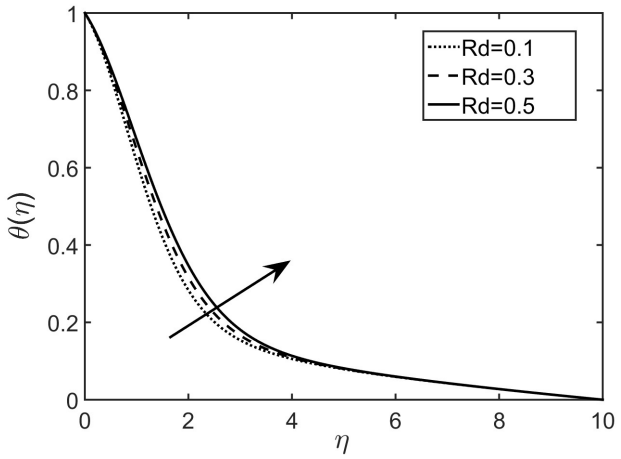

Figure 19**.** Variations of Temperature with the change in Radiation parameter.

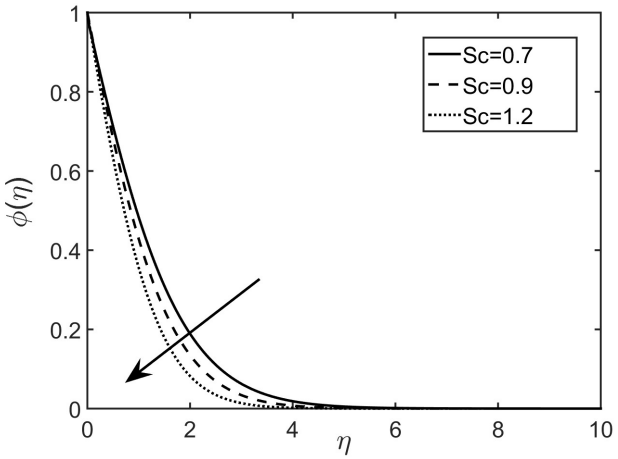

Figure 20**.** Variations of Concentration with the change in Schmidt number.

Inducing higher temperature profiles is the outcome of the frictional force that arises when the porosity parameter is raised. Presented in Fig. 15 are comprehensive temperature profiles of the Eckert number. Because of the Eckert number, its kinetic liveliness is moved into inside momentum when a force is applied to a viscous fluid in motion.Through viscous dissipation, the fluid's kinetic energy is converted into thermal energy by internal friction,

which results an increase in the liquid's warmth results from this cause. In Fig. 16, the Prandtl number is used to depict temperature patterns. If the Prandtl number is measured incrementally, the fluid's temperature will drop because its thermal conductivity will decrease. Figure 17 shows the heat source parameters' temperature profiles. Elevated temperatures result from a rise in the heat source parameter, which in turn generates heat in the fluid stream. Thermal conductivity parameter temperature profiles are indicated in Fig. 18. The heat outlines are affected by changes in the current border line sheet thickness, which is a measure of thermal conductivity. Figure 19 shows radiation parameter temperature profiles. The hotness spreading inside the liquid expands as the radiation parameter values go up because more heat is created. We can see the concentration profiles of the Schmidt number in Fig. 20.

Table 1. Values of the dimensionless Local Nusselt number $-\theta'(0)$ for various values of β, We, λ, ε, Ec, M, Q, J, and Fr.

$E1$	Δ	β	We	λ	ε	Ec	M	Q	J	Fr	$-\theta'(0)$
0.0	0.5	0.5	0.3	0.1	0.2	0.1	0.5	—	—	—	0.8018
0.1	—	—	—	—	—	—	—	—	—	—	0.8047
0.2	—	—	—	—	—	—	—	—	—	—	0.8067
0.2	0.1	—	—	—	—	—	—	—	—	—	0.8033
—	0.3	—	—	—	—	—	—	—	—	—	0.8067
—	0.5	—	—	—	—	—	—	—	—	—	0.8101
—	0.5	0.1	—	—	—	—	—	—	—	—	0.2479
—	—	0.3	—	—	—	—	—	—	—	—	0.7171
—	—	0.5	—	—	—	—	—	—	—	—	0.8101
—	—	0.5	0.1	—	—	—	—	—	—	—	0.8042
—	—	—	0.2	—	—	—	—	—	—	—	0.8072
—	—	—	0.3	—	—	—	—	—	—	—	0.8101
—	—	—	0.3	0.0	—	—	—	—	—	—	0.7770
—	—	—	—	0.1	—	—	—	—	—	—	0.8101
—	—	—	—	0.2	—	—	—	—	—	—	0.8338
—	—	—	—	0.1	0.0	—	—	—	—	—	0.8752
—	—	—	—	—	0.1	—	—	—	—	—	0.8397
—	—	—	—	—	0.2	—	—	—	—	—	00.8101
—	—	—	—	—	0.2	0.0	—	—	—	—	1.0198
—	—	—	—	—	—	0.1	—	—	—	—	0.8101
—	—	—	—	—	—	0.2	—	—	—	—	0.6016
—	—	—	—	—	—	0.2	0.1	—	—	—	0.5830
—	—	—	—	—	—	—	0.3	—	—	—	0.5923
—	—	—	—	—	—	—	0.5	—	—	—	0.6016
—	—	—	—	—	—	—	0.5	0.1	—	—	0.6016
—	—	—	—	—	—	—	—	0.3	—	—	0.4782
—	—	—	—	—	—	—	—	0.5	—	—	0.3485
—	—	—	—	—	—	—	—	0.1	0.1	—	0.6016
—	—	—	—	—	—	—	—	—	0.3	—	0.5358
—	—	—	—	—	—	—	—	—	0.5	—	0.4700
—	—	—	—	—	—	—	—	—	—	0.1	0.4679
—	—	—	—	—	—	—	—	—	—	0.4	0.5081
—	—	—	—	—	—	—	—	—	—	0.7	0.5457

A drop in concentration profiles is associated with a growth in dimension transference, which is shown in enhanced observations of the Schmidt number. Visualization of compound response factor focus patterns is portrayed in Fig. 21. All the figures are plotted with parameter values $\beta = 0.1$, $We = 0.3$, $E_1 = 0.1$, $M = 0.1$, $R = 0.3$, $Pr = 2$, $Ec = 0.5$, $k_p = 0.1$,$\Delta = 0.5$, $\varepsilon = 0.1$, $Sc = 0.6$, $\gamma = 0.1$. As the biological response consideration is studied more closely, it becomes clear that the chemical molecular diffusivity is decreasing, leading to decreased concentration profiles. Results for skin friction at changed Casson factor estimates are exhibited in Table 2, along with comparisons to the aforementioned literature. It is determined that the outcomes are satisfactory and the present numerical scheme shows high accuracy and strong consistency. In addition, we provide the results of the Nusselt number calculations for the different parameter affects in Table 1. It is observed that Nusselt number increases slightly for progressive values of Casson parameter. As Weissenberg number increases stronger elastic fields may occur so the Nusselt number increases. Increasing slip parameter enhancement heat transfer is noted. As porosity increases there is a significant increase in wall heat flux. For increasing observations of Eckert number heat transfer decreases so Nusselt number decreases. "The Casson-Williamson fluid has two competing rheological mechanisms."The Casson parameter introduces a yield stress that resists deformation while increasing effective viscosity in low-shear zones, limiting momentum transport and thickening the thermal and concentration boundary layers. In contrast, the Williamson parameter promotes shear-thinning by lowering viscosity in high shear regions (near the stretching surface) and increasing heat and mass transport. The overall transport behavior results from the interaction of both effects: yield stress suppresses convection while shear-thinning promotes it. As a result, the Casson parameter reduces the Nusselt and Sherwood numbers, but the Williamson parameter increases them.

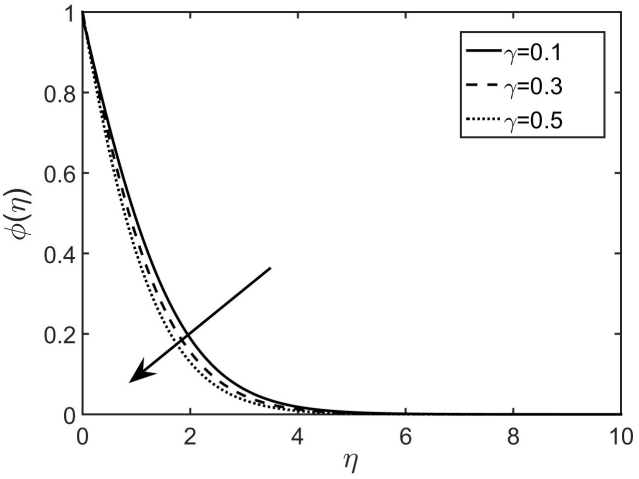

Figure 21**.** Variations of concentration with the change in the compound response constraint.

Table 2. Comparison the results of $-(1+\frac{1}{\beta})f''(0)$ with [29, 32].

β	Afify [32]	Abbas et al. [29]	Present Work	Error With [32]	Error with [29]
0.5	1.319520	1.319519	1.315609	0.2964	0.2963
4.0	0.846526	0.846526	0.846630	0.0123	0.0123
∞	0.776388	0.776388	0.776225	0.0210	0.0210

5. Conclusions

A constant two-dimensional Casson Williamson liquid flow is observed over an expanding sheet immersed in a permeable medium, influenced by magnetic and electric fields, Joule heating, and chemical reactions. The Keller Box numerical technique is utilized to simplify the partial differential equations governing the system. The influence of different parameters are examined by ploting profiles of velocity, temperature, and concentration. Consequently, the following conclusions are drawn.

- The velocity profiles drop when the Casson parameter, the magnetic parameter, the porous parameter, the Weissenberg number, and the velocity slip parameter are increased, whereas the electric field parameter decreases while the speed slip restriction is improved.An increase in the Casson parameter $\beta$from 0.1 to 0.5 leads to a 28% reduction in the velocity magnitude, indicating strong shear-thinning effects.An increase in the magnetic parameter M from 0.1 to 0.3 reduces the velocity by approximately 33%, demonstrating the strong braking effect of the Lorentz force. Increasing the permeability parameter κp from 1.0 to 2.0 reduces the velocity by approximately 36%, due to enhanced Darcy resistance in the porous medium.
- When the values of the Casson parameter, the magnetic field, the Eckert number, the porous restriction, the Weissenberg number, and the thermal conductivity are increased, the temperature profile is found to increase. On the other hand, when the Prandtl number is raised, the temperature profile has decreased. Increasing the Eckert number from $Ec = 0.2$ to $Ec = 0.6$ produces a noticeable rise in the temperature field. For example, at $\eta = 2$, the temperature increases from approximately $\theta(2) \approx 0.18(Ec = 0.2)$ to $\theta(2) \approx 0.32(Ec = 0.6)$, corresponding to a $\approx 78\%$ increase. Similarly, at $\eta = 3$, θ rises from $0.07(Ec = 0.2)$ to $0.14(Ec = 0.6)$, representing a 100% enhancement. This clearly confirms that viscous dissipation becomes more dominant at higher Ec values, resulting in a thicker thermal boundary layer and higher overall temperature.
- It has been observed that the concentration profiles decrease as the Schmidt number and substance response consideration are observed in sequential sequence. As the Schmidt number increases, the concentration boundary layer becomes thinner. For instance, at $\eta = 1$, the concentration decreases from $\phi(1) \approx 0.18$ for $Sc = 0.7$ to $\phi(1) \approx 0.11$ for $Sc = 1.2$, representing a $\approx 39\%$ reduction. Similarly, at $\eta = 2$, ϕ drops from about $0.05(Sc = 0.7)$ to $0.015(Sc = 1.2)$, corresponding to a 70% decrease. This confirms that higher Sc values—associated with lower mass diffusivity—lead to rapid concentration decay and a significantly thinner concentration boundary layer.
- Increasing slip parameter enhances Nusselt number values but opposes the flow of fluid consequently temperature upliftment is observed.
- For enhanced observations electric field, magnetic field parameters Nusselt number values increases.
- Finally The Casson-Williamson fluid model exhibits significant potential, particularly in interdisciplinary applications that merge non-Newtonian fluid dynamics with technology advancements. Also it has particular applications in thermal systems for improving thermal energy storage systems, modelling controlled flow of bio inks, biomedical engineering etc.
- In this paper we just studied the flow of Casson-Williamson fluid through Darcy Forchheimer permeable medium with the influence of Joule heating, chemical reaction influences. This study can be extended by using different boundary conditions and considering an entropy exploration study.

Authors' contribution

All authors contributed equally to the preparation of this article.

Declaration of competing interest

The authors declare no conflicts of interest.

Funding source

This study didn't receive any specific funds.

Data availability

The data that support the findings of this study are available from the corresponding author upon reasonable request.

REFERENCES

[1] K. Vajravelu, S. Sreenadh, R. H. Reddy, and K. Murugesan, "Peristaltic transport of a casson fluid in contact with a newtonian fluid in a circular tube with permeable wall," *International Journal of Fluid Mechanics Research*, vol. 36, no. 3, pp. 244–254, 2009. [Online]. Available: https://doi.org/10.1615/InterJFluidMechRes.v36.i3.40

[2] M. Mustafa, T. Hayat, I. Pop, and A. Aziz, "Unsteady boundary layer flow of a casson fluid due to an impulsively started moving flat plate," *Heat Transfer—Asian Research*, vol. 40, no. 6, pp. 563–576, 2011. [Online]. Available: https://doi.org/10.1002/htj.20358

[3] S. Mukhopadhyay, K. Vajravelu, and R. A. Van Gorder, "Casson fluid flow and heat transfer at an exponentially stretching permeable surface," *Journal of Applied Mechanics*, vol. 80, no. 5, p. 054502, 07 2013. [Online]. Available: https://doi.org/10.1115/1.4023618

[4] G. Makanda, S. Shaw, and P. Sibanda, "Diffusion of chemically reactive species in casson fluid flow over an unsteady stretching surface in porous medium in the presence of a magnetic field," *Mathematical Problems in Engineering*, vol. 2015, no. 1, p. 724596, 2015. [Online]. Available: https://doi.org/10.1155/2015/724596

[5] K. Pushpalath, S. Vangala, J. V. Ramana Reddy, and D. Sandeep, "Heat and mass transfer in unsteady mhd casson fluid flow with convective boundary conditions," *International Journal of Advanced Science and Technology*, vol. 91, pp. 19–38, 07 2016. [Online]. Available: https://doi.org/10.14257/ijast.2016.91.03

[6] S. Nadeem and S. Hussain, "Heat transfer analysis of williamson fluid over exponentially stretching surface," *Applied Mathematics and Mechanics*, vol. 35, pp. 489–502, 04 2014. [Online]. Available: https://doi.org/10.1007/s10483-014-1807-6

[7] T. Hayat, A. Shafiq, and A. Alsaedi, "Hydromagnetic boundary layer flow of williamson fluid in the presence of thermal radiation and ohmic dissipation," *Alexandria Engineering Journal*, vol. 55, no. 3, pp. 2229–2240, 2016. [Online]. Available: https://doi.org/10.1016/j.aej.2016.06.004

[8] A. Megahed, "Williamson fluid flow due to a nonlinearly stretching sheet with viscous dissipation and thermal radiation," *Journal of the Egyptian Mathematical Society*, vol. 27, p. 12, 06 2019. [Online]. Available: https://doi.org/10.1186/s42787-019-0016-y

[9] M. Ramzan, S. Rehman, M. S. Junaid, A. Saeed, P. Kumam, and W. Watthayu, "Dynamics of williamson ferro-nanofluid due to bioconvection in the portfolio of magnetic dipole and activation energy over a stretching sheet," *International Communications in Heat and Mass Transfer*, vol. 137, p. 106245, 2022. [Online]. Available: https://doi.org/10.1016/j.icheatmasstransfer.2022.106245

[10] A. Zhu, H. Ali, M. Ishaq, M. S. Junaid, J. Raza, and M. Amjad, "Numerical study of heat and mass transfer for williamson nanofluid over stretching/shrinking sheet along with brownian and thermophoresis effects," *Energies*, vol. 15, no. 16, 2022. [Online]. Available: https://www.mdpi.com/1996-1073/15/16/5926

[11] P. Priyadharshini, V. Karpagam, N. A. Shah, and M. H. Alshehri, "Bioconvection effects of mhd williamson fluid flow over a symmetrically stretching sheet: Machine learning," *Symmetry*, vol. 15, no. 9, 2023. [Online]. Available: https://www.mdpi.com/2073-8994/15/9/1684

[12] M. S. Arif, W. Shatanawi, and Y. Nawaz, "Finite element study of electrical mhd williamson nanofluid flow under the effects of frictional heating in the view of viscous dissipation," *Energies*, vol. 16, no. 6, 2023. [Online]. Available: https://www.mdpi.com/1996-1073/16/6/2778

[13] P. Kumar, B. Nagaraja, F. Almeida, D. Ar, Q. Al-Mdallal, and F. Jarad, "Magnetic dipole effects on unsteady flow of casson-williamson nanofluid propelled by stretching slippery curved melting sheet with buoyancy force," *Scientific Reports*, vol. 13, 08 2023. [Online]. Available: https://doi.org/10.1038/s41598-023-39354-5

[14] R. Kumar, R. Durga Rao, and V. Murthy, "Characteristics of williamson-casson-nanofluid flow across an impermeable extending the sheet in the

existingof heat transfer melting and electromagnetic field," *Dongbei Daxue Xuebao/Journal of Northeastern University*, vol. 25, pp. 1853–1874, 12 2022.

[15] N. Yousef, A. M. Megahed, N. I. Ghoneim, M. Elsafi, and E. Fares, "Chemical reaction impact on mhd dissipative casson-williamson nanofluid flow over a slippery stretching sheet through porous medium," *Alexandria Engineering Journal*, vol. 61, no. 12, pp. 10 161–10 170, 2022. [Online]. Available: https://doi.org/10.1016/j.aej.2022.03.032

[16] O. Kazaz and E. Abu-Nada, "Innovative high-energy nanocomposite absorbers for superior solar-driven water desalination through broadband solar energy harvesting," *Applied Thermal Engineering*, vol. 273, p. 126531, 2025. [Online]. Available: https://doi.org/10.1016/j.applthermaleng.2025.126531

[17] A. M. Hassan, M. A. Alomari, A. Alajmi, A. M. Sadeq, F. Alqurashi, M. A. Flayyih, and O. Kazaz, "Numerical analysis of coupled fluid-structure interaction in magnetohydrodynamic flow and phase change process of nano-encapsulated phase change material systems with deformable heated surface," *Case Studies in Thermal Engineering*, vol. 70, p. 106131, 2025. [Online]. Available: https://doi.org/10.1016/j.csite.2025.106131

[18] O. Kazaz and E. Abu-Nada, "Thermal performance of nano-architected phase change energetic materials for a next-generation solar harvesting system," *Energy Conversion and Management*, vol. 327, p. 119541, 2025. [Online]. Available: https://doi.org/10.1016/j.enconman.2025.119541

[19] M. Nazeer, A. Al-Zubaidi, F. Hussain, F. Z. Duraihem, S. Anila, and S. Saleem, "Thermal transport of two-phase physiological flow of non-newtonian fluid through an inclined channel with flexible walls," *Case Studies in Thermal Engineering*, vol. 35, p. 102146, 2022. [Online]. Available: https://doi.org/10.1016/j.csite.2022.102146

[20] F. Hussain, M. Nazeer, M. Altanji, A. Saleem, and M. Ghafar, "Thermal analysis of casson rheological fluid with gold nanoparticles under the impact of gravitational and magnetic forces," *Case Studies in Thermal Engineering*, vol. 28, p. 101433, 2021. [Online]. Available: https://doi.org/10.1016/j.csite.2021.101433

[21] S. Saleem, F. Hussain, M. Irfan, I. Siddique, M. Nazeer, and S. Eldin, "Theoretical investigation of heat transfer analysis in ellis nanofluid flow through the divergent channel," *Case Studies in Thermal Engineering*, vol. 48, p. 103140, 2023. [Online]. Available: https://doi.org/10.1016/j.csite.2023.103140

[22] M. Irfan, I. Siddique, M. Nazeer, S. Saleem, and N. Radwan, "Heat transfer analysis of single-walled carbon nanotubes in ellis's fluid model: Comparative study of uniform and non-uniform channels," *Case Studies in Thermal Engineering*, vol. 54, p. 104036, 2024. [Online]. Available: https://doi.org/10.1016/j.csite.2024.104036

[23] A. Islam, Z. Mahmood, U. Khan, B. Ali, and M. I. H. Siddiqui, "Joule heating effects on triple diffusive free convective mhd flow over a convective surface: A lie-group transformation analysis," *Modern Physics Letters B*, vol. 39, no. 03, p. 2450412, 2025. [Online]. Available: https://doi.org/10.1142/S0217984924504128

[24] M. Nazeer, S. Almohammadi, N. Radwan, and W. Ahmad, "Heat transfer analysis in hydromagnetic two-phase williamson fluid through tilted channel: Applications of gold and silver nanoparticles in solar thermal energy," *ZAMM - Journal of Applied Mathematics and Mechanics*, vol. 105, 01 2025. [Online]. Available: https://doi.org/10.1002/zamm.202400397

[25] M. Nazeer, M. Irfan, F. Hussain, and I. Siddique, "Entropy generation analysis in blood-gold casson nanofluid through horizontal wavy channel with velocity and thermal slips: Applications in skin diseases," *Journal of Computational Biophysics and Chemistry*, vol. 22, no. 03, pp. 259–272, 2023. [Online]. Available: https://doi.org/10.1142/S2737416523400021

[26] S. Almutairi, F. Hussain, M. Nazeer, S. Saleem, and R. S. Mohammed, "Perturbation solution of multiphase flow of williamson fluid through convergent and divergent conduits: Electro-osmotic effects," *Modern Physics Letters B*, vol. 38, no. 34, p. 2450348, 2024. [Online]. Available: https://doi.org/10.1142/S0217984924503482

[27] M. Irfan, M. Nazeer, F. Hussain, and I. Siddique, "Heat transfer analysis in the peristaltic flow of casson nanofluid through asymmetric channel with velocity and thermal slips: Applications in a complex system," *International Journal of Modern Physics B*, vol. 36, no. 32, p. 2250231, 2022. [Online]. Available: https://doi.org/10.1142/S0217979222502319

[28] F. Hussain, M. Nazeer, I. Ghafoor, A. Saleem, B. Waris, and I. Siddique, "Perturbation solution of couette flow of casson nano-fluid with composite porous medium inside a vertical channel," *Nanoscience and Technology: An International Journal*, vol. 13, 01 2022. [Online]. Available: https://doi.org/10.1615/NanoSciTechnolIntJ.2022038799

[29] W. Abbas, A. Megahed, M. Ibrahim, and A. Said, "Ohmic dissipation impact on flow of casson-williamson fluid over a slippery surface through a porous medium," *Indian Journal of Physics*, vol. 97, pp. 4277–4283, 05 2023. [Online]. Available: https://doi.org/10.1007/s12648-023-02754-4

[30] M. A. Alomari, A. M. Hassan, Q. H. Al-Salami, F. Q. Alyousuf, F. Alqurashi, and M. A. Flayyih, "Convection flow of ne-phase change material-water mixture in evacuated tube solar collector manifold: Numerical analysis of mhd double-diffusive convection and exothermic reaction," *International Communications in Heat and Mass Transfer*, vol. 159, p. 108194, 2024. [Online]. Available: https://doi.org/10.1016/j.icheatmasstransfer.2024.108194

[31] B. Ali, U. Ishtiaq, I.-L. Popa, H. A. El-Wahed Khalifa, A. Kumar, and M. I. Haque Siddiqui, "Numerical modelling and deep learning-based analysis of unsteady micropolar nanofluid flow with heat radiation over a riga plate," *Journal of Radiation Research and Applied Sciences*, vol. 18, no. 2, p. 101512, 2025. [Online]. Available: https://doi.org/10.1016/j.jrras.2025.101512

[32] A. Afify, "The influence of slip boundary condition on casson nanofluid flow over a stretching sheet in the presence of viscous dissipation and chemical reaction," *Mathematical Problems in Engineering*, vol. 2017, pp. 1–12, 07 2017. [Online]. Available: https://doi.org/10.1155/2017/3804751

How to cite this article:
Vardireddy Sujatha, Wuriti Sridhar, Mohammed Abu-Ghurban, Ganugapati R. Ganesh, G. Dharmaiah, (2026). 'Insights of Joule heating and chemical reaction effects on Casson-Williamson fluid in a thermally active Darcy–Forchheimer medium', Al-Qadisiyah Journal for Engineering Sciences, 19(1), pp. 153- 163.
https://doi.org/10.30772/qjes.2025.165491.1749